Applied Physics Express

The Japan Society of Applied Physics

LETTERS

Low-pressure CVD-grown β-Ga_2O_3 bevel-field-plated Schottky barrier diodes

To cite this article: Chandan Joishi *et al* 2018 *Appl. Phys. Express* **11** 031101

View the article online for updates and enhancements.

Related content

- Nearly ideal vertical GaN Schottky barrier diodes with ultralow turn-on voltage and on-resistance
Bing Ren, Meiyong Liao, Masatomo Sumiya et al.

- State-of-the-art technologies of gallium oxide power devices
Masataka Higashiwaki, Akito Kuramata, Hisashi Murakami et al.

- Recent progress in Ga2O3 power devices
Masataka Higashiwaki, Kohei Sasaki, Hisashi Murakami et al.

This content was downloaded from IP address 128.146.164.241 on 21/02/2018 at 20:25

Applied Physics Express **11**, 031101 (2018)
https://doi.org/10.7567/APEX.11.031101

CrossMark

Low-pressure CVD-grown β-Ga_2O_3 bevel-field-plated Schottky barrier diodes

Chandan Joishi[1,2*], Subrina Rafique[1,3], Zhanbo Xia[1], Lu Han[3], Sriram Krishnamoorthy[1,4], Yuewei Zhang[1], Saurabh Lodha[2], Hongping Zhao[1,3,5], and Siddharth Rajan[1,5*]

[1]*Department of Electrical and Computer Engineering, The Ohio State University, Columbus, OH 43210, U.S.A.*
[2]*Department of Electrical Engineering, Indian Institute of Technology Bombay, Mumbai, Maharashtra 400076, India*
[3]*Department of Electrical Engineering and Computer Science, Case Western Reserve University, Cleveland, OH 44106, U.S.A.*
[4]*Department of Electrical and Computer Engineering, The University of Utah, Salt Lake City, UT 84112, U.S.A.*
[5]*Department of Materials Science and Engineering, The Ohio State University, Columbus, OH 43210, U.S.A.*

*E-mail: cjnits@gmail.com; rajan.21@osu.edu

Received December 22, 2017; accepted January 26, 2018; published online February 14, 2018

We report (010)-oriented β-Ga_2O_3 bevel-field-plated mesa Schottky barrier diodes grown by low-pressure chemical vapor deposition (LPCVD) using a solid Ga precursor and O_2 and $SiCl_4$ sources. Schottky diodes with good ideality and low reverse leakage were realized on the epitaxial material. Edge termination using beveled field plates yielded a breakdown voltage of −190 V, and maximum vertical electric fields of 4.2 MV/cm in the center and 5.9 MV/cm at the edge were estimated, with extrinsic R_{ON} of 3.9 mΩ·cm^2 and extracted intrinsic R_{ON} of 0.023 mΩ·cm^2. The reported results demonstrate the high quality of homoepitaxial LPCVD-grown β-Ga_2O_3 thin films for vertical power electronics applications, and show that this growth method is promising for future β-Ga_2O_3 technology. © 2018 The Japan Society of Applied Physics

β-Ga_2O_3 is an ultra-wide bandgap semiconductor with a room-temperature bandgap of 4.5–4.9 eV[1,2] and an estimated breakdown field of 6–8 MV/cm.[3] Its high breakdown field leads to large theoretical figures of merit for power switching,[4] with a lower expected on-resistance (R_{ON})[3–5] for a given breakdown voltage (V_{BR}) than those of incumbent wide bandgap materials such as SiC and GaN. The availability of large-area, high-quality native Ga_2O_3 substrates prepared by scalable and low-cost melt-grown techniques[6–10] make Ga_2O_3-based power devices promising for technological insertion in high-power systems. Lateral devices such as field-effect transistors[11–18] and vertical devices including Schottky rectifiers[19–25] and trench MOSFETs[26–28] have been recently demonstrated by various groups using both β- and α-Ga_2O_3.[29]

Vertical devices are preferred over lateral geometries for high-power applications, but vertical device topologies require an epitaxial growth technology capable of growing thick and low-doped drift layers. Several growth techniques, including molecular beam epitaxy[30–32] (MBE), pulsed layer deposition[33] (PLD), mist-CVD,[29] atmospheric-pressure CVD[34] (APCVD), low-pressure CVD[35,36] (LPCVD), halide vapor phase epitaxy[37] (HVPE), and metal organic chemical vapor deposition[38,39] (MOCVD), have been demonstrated for the growth of β-Ga_2O_3. HVPE with a growth rate of 5 µm/h on (001)[37] and LPCVD with a growth rate of ∼2 µm/h on (010) substrates[36] are two demonstrated homoepitaxial growth technologies with relatively high growth rates. In addition, LPCVD provides a low-cost solution for growing high-quality epitaxial Ga_2O_3 with controllable doping[40] and high electron mobility compared with other present techniques. Using HVPE, Schottky diodes with planar field-plate termination[23] exhibiting breakdown voltage greater than 1 kV have already been demonstrated. However, there are no reports to date on Schottky diodes fabricated using LPCVD-grown β-Ga_2O_3 films. In this work, we have fabricated Schottky diodes to verify the material quality and investigate device performance in order to demonstrate the viability of LPCVD as a growth technique for vertical power electronic devices. The fabricated diode exhibits a breakdown field (F_{BR}) of 4.2 MV/cm, extrinsic R_{ON} of 3.9 mΩ·cm^2, and extracted intrinsic R_{ON} of 0.023 mΩ·cm^2. The extracted F_{BR} is higher than the theoretical F_{BR} values for 4H-SiC (2.2 MV/cm)[41] and GaN (3.3 MV/cm).[41] The high-performance devices obtained on LPCVD-grown layers demonstrate the potential of this growth method for future β-Ga_2O_3 technology.

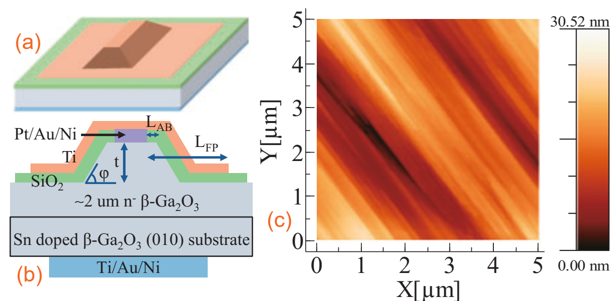

Fig. 1. (a) 3D schematic of the fabricated Schottky barrier diode. (b) 2D cross schematic highlighting the epitaxial stack, the contacts, and field plate. L_{FP} (∼4 µm) is the field-plate overlap and L_{AB} (0.25 µm) is the anode-bevel extension. (c) AFM image for the as-grown β-Ga_2O_3 film by LPCVD.

A three-dimensional representation of the fabricated beveled field-plate Schottky diode is shown in Fig. 1(a), along with its cross-sectional schematic in Fig. 1(b). The epitaxial stack consists of ∼2 µm β-Ga_2O_3 thin film grown by LPCVD on commercially available Sn-doped (010) β-Ga_2O_3 substrates.[43] Growth was carried out in a horizontal furnace with programmable temperature and precise pressure controllers. A growth temperature of 900 °C and a pressure of 4 Torr were used, leading to a nominal growth rate of 2 µm/h. Pregrowth sample preparation involved solvent cleaning using acetone, toluene, and isopropyl alcohol, followed by an N_2 blow-dry. Prior to the growth, the samples were annealed in situ at 900 °C for 30 min in O_2 ambient. High-purity gallium pellets (Alfa Aesar, 99.99999%) and O_2 were used as the source materials and argon (Ar) was used as the carrier gas. Silicon tetrachloride ($SiCl_4$) was used as the n-type dopant source. Atomic force microscopy (AFM) on the sample surface after growth showed a root-mean-square (rms) surface roughness (t_{rms}) of 4.86 nm, as seen in Fig. 1(c).

i-Line stepper lithography was used in the processing of the diodes. The diode fabrication commenced with the deposition of the anode (Pt/Au/Ni) using an e-beam evaporator

 © 2018 The Japan Society of Applied Physics

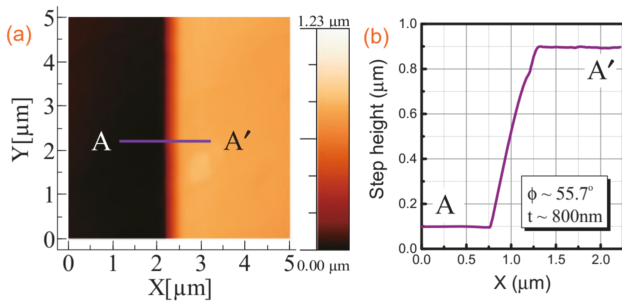

Fig. 2. (a) AFM image for trench analysis. (b) Measured step profile and bevel (slant) angle along the cutline (AA′).

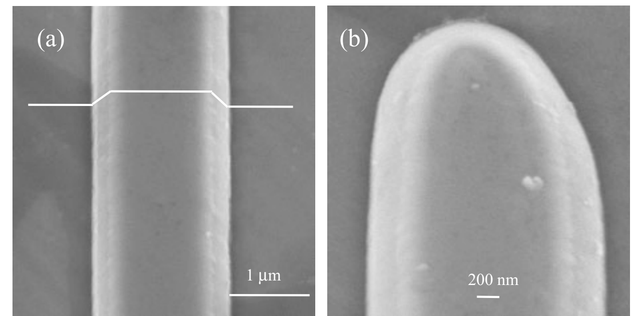

Fig. 3. SEM images of (a) center portion of the diode after field-plate fabrication and (b) one edge of the diode showing inclined curvature.

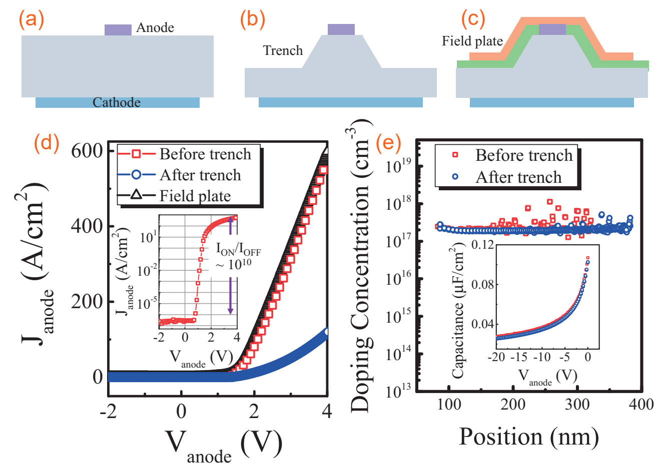

Fig. 4. (a) Before trench etching, (b) after trench etching, and (c) field-plate Schottky diode schematics. (d) *J*–*V* characteristics of the device at different stages of the diode process with log plot for the device before trench etching in the inset. (e) Charge profile plot along with *C*–*V* curves in the inset.

with Pt as the work function metal. The anode electrode in the devices discussed here is a stripe [Fig. 1(a)] of 50 µm length and 1 µm width designed with rounded corners to avoid breakdown voltage degradation due to the formation of spherical junctions.[42] The cathode ohmic contact was deposited on the back of the substrate using e-beam-deposited Ti/Au/Ni. Bevel/trench patterns were formed, which covered the anode metal and extended nominally 0.25 µm from the anode edge on all sides. The device breakdown just after the formation of the anode and cathode was achieved at a depletion width of ~0.8 µm; hence, the anode-bevel extension (L_{AB}) was chosen as 0.25 µm (<0.8 µm) to leverage the advantages of a bevel design.[42] Further details of the device simulation and design are provided later. Subsequently, dry etching to form the trench was carried out in a Plasma-Therm SLR 770 ICP-RIE system using BCl_3/Ar gas flow of 35/5 sccm, 30 W RIE, 200 W ICP, and 5 mTorr chamber pressure. In previous studies, dry etching using BCl_3 was shown to result in an inclined profile.[44] AFM was used to measure the etch depth (t) and the bevel angle (φ) as ~800 nm and ~56°, respectively (Fig. 2). Thereafter, 300 nm of SiO_2 was deposited conformally by plasma-enhanced CVD (PECVD) at 250 °C as a surface passivation layer. A SiO_2 thickness of 300 nm was chosen on the basis of the results of two-dimensional simulations using Silvaco ATLAS to target F_{BR} ~5 MV/cm. To form the metal field-plate, the oxide layer on top of the anode metal was etched away to form a contact between the anode and the metal plate deposited by conformal sputtering of Ti. Finally, the field plates with a field-plate overlap (L_{FP}) of ~4 µm were patterned with the remaining metal being etched using dilute hydrochloric acid (HCl) at 65 °C. Figure 3(a) shows the scanning electron microscopy (SEM) images of the diode after field-plate integration where the beveled profile is distinct. Figure 3(b) shows the SEM image for one end of the diode along its length with the rounded pattern designed to avoid sharp corners.

Electrical characteristics were measured using an Agilent B1500A semiconductor device analyzer. Room-temperature current–voltage (*J*–*V*) characteristics of the device are shown in Fig. 4(a). The anode current density vs voltage curves were plotted and compared for the following three structures: (a) after the formation of anode and cathode electrodes and before trench etching, (b) after trench etching and before the deposition of SiO_2, and (c) after the final fabrication step. An ideality factor (η) of 1.03 ± 0.02, a high I_{ON}/I_{OFF} ratio of ~10^{10}, and a specific on-resistance (R_{ON}) of 3.6 mΩ·cm^2 were calculated before trench etching. I_{ON} for the diode decreases after BCl_3/Ar etching, accompanied by increases in R_{ON} to 6.7 mΩ·cm^2 and η to 1.1 ± 0.03. We believe that the increase in resistance is related to surface damage that is subsequently repaired during the passivation. The mechanism of this is not understood at present. This is similar to previous reports on BCl_3/Ar etching being unfavorable for Schottky diodes.[45] With the formation of the field plate, R_{ON} decreased to 3.9 mΩ·cm^2, and similar characteristics to those before trench etching were obtained, suggesting that the surface damage caused by BCl_3/Ar etching was passivated by the SiO_2. Figure 4(b) shows the charge profiles before and after trench etching as a function of the depletion width. A doping density (N_D) of 2.5×10^{17} cm^{-3} was obtained from capacitance–voltage (*C*–*V*) measurements (the *C*–*V* characteristics from which the corresponding charge profiles were extracted are shown in the inset). The measured charge density was similar before and after trench etching, suggesting that while BCl_3/Ar etching results in damage of the sidewall surface, it does not cause significant charge depletion. The *C*–*V* plot after the formation of the field plate includes contributions from the Ti/SiO_2/Ga_2O_3 (metal oxide semiconductor) sidewall and bond-pad regions, and is therefore not shown here.

Figure 5(a) shows the two-terminal reverse current breakdown characteristics for identical, fresh devices at various stages of the process, with immersion in Fluorinert[46] to

 © 2018 The Japan Society of Applied Physics

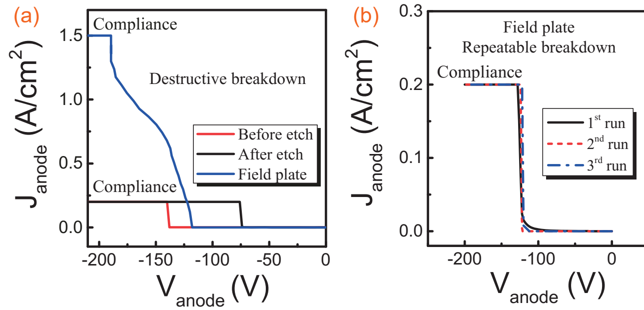

Fig. 5. (a) Two-terminal destructive reverse breakdown characteristics. (b) Nondestructive breakdown for the field-plated device.

prevent air breakdown. An anode current compliance of 0.2 A/cm^2 (3–4 orders of magnitude lower than I_{ON}) is seen to cause destructive breakdown with a breakdown voltage (V_{BR}) of −138 V for diodes before trench etching and −74 V after trench etching. This indicates that the expected enhancement in breakdown voltage using a bevel edge-termination design was not obtained after BCl_3/Ar etching. Further analysis is needed to understand this, but one possible reason could be the surface damage caused by BCl_3/Ar etching,[45] which leads to surface-related leakage. By fabricating the field-plate structure on top of the "after trench" device, V_{BR} was increased from −74 to −190 V. Field-plated Schottky diodes were also found to withstand one order higher current density (>1 A/cm^2) before breaking down catastrophically.

The reverse current seen in the curve after −130 V was deduced to be leakage current through SiO_2, which adds to the overall current. Setting a current compliance of 0.2 A/cm^2 for the field plates resulted in repeatable breakdown [Fig. 5(b)] with $V_{BR} = -129$ V. The measured V_{BR} values, Schottky contact barrier height (1.5 eV), and doping density (both extracted from the *C*–*V* data) were used to calculate the depletion width (W_{dep}) and peak electric field (F_{max}) using one-dimensional Poisson's equation. W_{dep} of 0.8 µm, which corresponds to F_{max} of 3.5 MV/cm, was estimated for the device before trench etching. Since W_{dep} of 0.8 µm is less than the epitaxial layer thickness (~2 µm), this corresponds to non-punch-through breakdown of the devices. Two-dimensional device simulations using Silvaco ATLAS were used to estimate the electric field at the center of the diode, as shown in Fig. 6(b). The foot edge of the anode shows a peak field higher than the theoretical Ga_2O_3 breakdown field (8 MV/cm), similar to a previous report.[23] The corresponding W_{dep} and F_{max} values for the device after trench etching decreased to 0.65 µm and 2.4 MV/cm, respectively. With the field plate, F_{max} of 3.4 MV/cm for repeatable breakdown and 4.2 MV/cm for destructive breakdown were calculated (i.e., F_{max} increased from 2.4 MV/cm after trench etching to 4.2 MV/cm after field-plate insertion). 2D Silvaco simulations for destructive breakdown on the field plate were seen to match the calculated 4.2 MV/cm field at the center of the diode with the peak field of 5.9 MV/cm at the corner. The calculated values of W_{dep} and F_{max} are tabulated in Table I. The last column in the table lists the intrinsic R_{ON} values for all N_D and W_{dep} values estimated using the equation

$$R_{ON} = \frac{W_{dep}}{qN_D\mu},$$

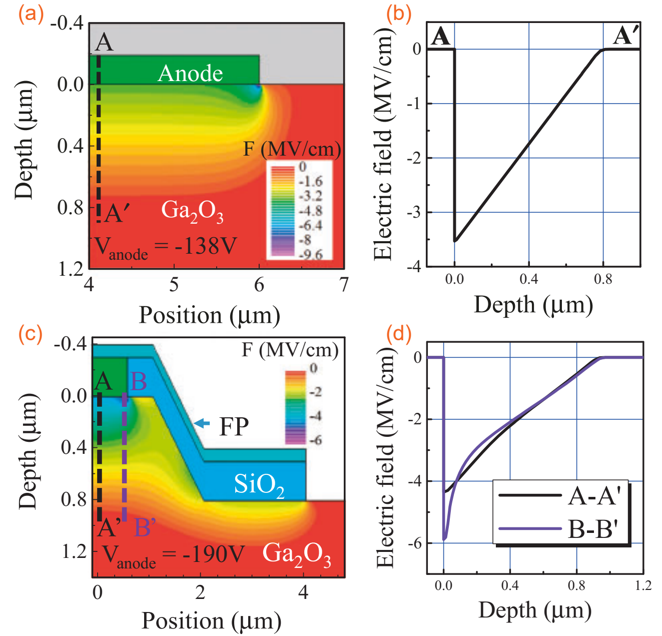

Fig. 6. (a) 2D Silvaco ATLAS simulations to highlight vertical electric field (F) contour map in Ga_2O_3 (a) before trench etching and (c) after field-plate (FP) insertion. (b) and (d) Measured field magnitudes along the cutlines.

Table I. All the experimental V_{BR} values and corresponding calculated W_{dep}, F_{max}, and R_{ON}.

Diode structure		V_{BR} (V)	W_{dep} (µm)	F_{max} (MV/cm)	R_{ON} (mΩ·cm^2)
Before trench		−138	0.80	3.5	0.019
After trench		−74	0.65	2.4	0.020
Field plate	BD1	−190	0.92	4.2	0.023
	BD2	−129	0.76	3.4	0.019

BD1: Destructive breakdown
BD2: Repeatable breakdown for the field-plated diodes

where $q = 1.6 \times 10^{-19}$ C is the elementary electric charge and μ is the mobility (~100 cm^2 V^{-1} s^{-1}, estimated from the Hall measurement of in-plane mobility). As expected for a back contact, the measured device resistance is dominated by the extrinsic resistance of the substrate.

In summary, we demonstrated a field-plate bevel mesa Schottky diode using LPCVD-grown β-Ga_2O_3 thin film. A high breakdown field of 4.2 MV/cm, extrinsic R_{ON} of 3.9 mΩ·cm^2, and intrinsic R_{ON} of 0.023 mΩ·cm^2 were estimated for the devices, indicating the high quality of the LPCVD-grown layers. Device performance degradation due to BCl_3/Ar was mitigated by SiO_2 passivation. Future developments in epitaxial growth for lower background doping and field management will enable β-Ga_2O_3 power devices with lower conduction and switching losses. The reported work shows the promise of LPCVD β-Ga_2O_3 for low-cost high-power devices.

Acknowledgments We acknowledge funding from the Department of Defense, Defense Threat Reduction Agency (Grant HDTRA11710034), National Science Foundation (DMR-1755479), ONR EXEDE MURI program, and the OSU Institute for Materials Research Seed Program. We thank the Air Force Research Laboratory (D. Dorsey, G. Jessen, and K. Chabak) for support. The content of the information does not necessarily reflect the position or the policy of the federal government, and no official endorsement should be inferred.

© 2018 The Japan Society of Applied Physics

1) H. H. Tippins, Phys. Rev. **140**, A316 (1965).
2) M. R. Lorenz, J. F. Woods, and R. J. Gambino, J. Phys. Chem. Solids **28**, 403 (1967).
3) M. Higashiwaki, K. Sasaki, A. Kuramata, T. Masui, and S. Yamakoshi, Appl. Phys. Lett. **100**, 013504 (2012).
4) B. J. Baliga, J. Appl. Phys. **53**, 1759 (1982).
5) M. Higashiwaki, K. Sasaki, A. Kuramata, T. Masui, and S. Yamakoshi, Phys. Status Solidi A **211**, 21 (2014).
6) Z. Galazka, R. Uecker, K. Irmscher, M. Albrecht, D. Klimm, M. Pietsch, M. Brützam, R. Bertram, S. Ganschow, and R. Fornari, Cryst. Res. Technol. **45**, 1229 (2010).
7) K. Irmscher, Z. Galazka, M. Pietsch, R. Uecker, and R. Fornari, J. Appl. Phys. **110**, 063720 (2011).
8) H. Aida, K. Nishiguchi, H. Takeda, N. Aota, K. Sunakawa, and Y. Yaguchi, Jpn. J. Appl. Phys. **47**, 8506 (2008).
9) E. G. Víllora, K. Shimamura, Y. Yoshikawa, T. Ujiie, and K. Aoki, Appl. Phys. Lett. **92**, 202120 (2008).
10) J. Zhang, B. Li, C. Xia, G. Pei, Q. Deng, Z. Yang, W. Xu, H. Shi, F. Wu, Y. Wu, and J. Xu, J. Phys. Chem. Solids **67**, 2448 (2006).
11) M. Higashiwaki, K. Sasaki, T. Kamimura, M. H. Wong, D. Krishnamurthy, A. Kuramata, T. Masui, and S. Yamakoshi, Appl. Phys. Lett. **103**, 123511 (2013).
12) M. H. Wong, K. Sasaki, A. Kuramata, S. Yamakoshi, and M. Higashiwaki, IEEE Electron Device Lett. **37**, 212 (2016).
13) A. J. Green, K. D. Chabak, E. R. Heller, R. C. Fitch, M. Baldini, A. Fiedler, K. Irmscher, G. Wagner, Z. Galazka, S. E. Tetlak, A. Crespo, K. Leedy, and G. H. Jessen, IEEE Electron Device Lett. **37**, 902 (2016).
14) W. S. Hwang, A. Verma, H. Peelaers, V. Protasenko, S. Rouvimov, H. Xing, A. Seabaugh, W. Haensch, C. Van de Walle, Z. Galazka, M. Albrecht, R. Fornari, and D. Jena, Appl. Phys. Lett. **104**, 203111 (2014).
15) H. Zhou, K. Maize, G. Qiu, A. Shakouri, and P. D. Ye, arXiv:1703.06197.
16) K. D. Chabak, N. Moser, A. J. Green, D. E. Walker, Jr., S. E. Tetlak, E. Heller, A. Crespo, R. Fitch, J. P. McCandless, K. Leedy, M. Baldini, G. Wagner, Z. Galazka, X. Li, and G. Jessen, Appl. Phys. Lett. **109**, 213501 (2016).
17) S. Krishnamoorthy, Z. Xia, C. Joishi, Y. Zhang, J. McGlone, J. Johnson, M. Brenner, A. R. Arehart, J. Hwang, S. Lodha, and S. Rajan, Appl. Phys. Lett. **111**, 023502 (2017).
18) S. Krishnamoorthy, Z. Xia, S. Bajaj, M. Brenner, and S. Rajan, Appl. Phys. Express **10**, 051102 (2017).
19) K. Sasaki, M. Higashiwaki, A. Kuramata, T. Masui, and S. Yamakoshi, IEEE Electron Device Lett. **34**, 493 (2013).
20) M. Oda, R. Tokuda, H. Kambara, T. Tanikawa, T. Sasaki, and T. Hitora, Appl. Phys. Express **9**, 021101 (2016).
21) T. Oishi, Y. Koga, K. Harada, and M. Kasu, Appl. Phys. Express **8**, 031101 (2015).
22) M. Higashiwaki, K. Konishi, K. Sasaki, K. Goto, K. Nomura, Q. T. Thieu, R. Togashi, H. Murakami, Y. Kumagai, B. Monemar, A. Koukitu, A. Kuramata, and S. Yamakoshi, Appl. Phys. Lett. **108**, 133503 (2016).
23) K. Konishi, K. Goto, H. Murakami, Y. Kumagai, A. Kuramata, S. Yamakoshi, and M. Higashiwaki, Appl. Phys. Lett. **110**, 103506 (2017).
24) J. Yang, S. Ahn, F. Ren, S. J. Pearton, S. Jang, J. Kim, and A. Kuramata, Appl. Phys. Lett. **110**, 192101 (2017).
25) K. Sasaki, D. Wakimoto, Q. T. Thieu, Y. Koishikawa, A. Kuramata, M. Higashiwaki, and S. Yamakoshi, IEEE Electron Device Lett. **38**, 783 (2017).
26) K. Sasaki, Q. T. Thieu, D. Wakimoto, Y. Koishikawa, A. Kuramata, and S. Yamakoshi, Appl. Phys. Express **10**, 124201 (2017).
27) Z. Hu, K. Nomoto, W. Li, L. J. Zhang, J.-H. Shin, N. Tanen, T. Nakamura, D. Jena, and H. G. Xing, 75th Annu. Device Research Conf. (DRC), 2017, p. 1.
28) M. H. Wong, K. Goto, A. Kuramata, S. Yamakoshi, H. Murakami, Y. Kumagai, and M. Higashiwaki, 75th Annu. Device Research Conf. (DRC), 2017, p. 1.
29) D. Shinohara and S. Fujita, Jpn. J. Appl. Phys. **47**, 7311 (2008).
30) K. Sasaki, A. Kuramata, T. Masui, E. G. Víllora, K. Shimamura, and S. Yamakoshi, Appl. Phys. Express **5**, 035502 (2012).
31) E. Ahmadi, O. S. Kokaldi, S. W. Kaun, Y. Oshima, D. B. Short, U. K. Mishra, and J. S. Speck, Appl. Phys. Express **10**, 041102 (2017).
32) T. Oshima, T. Okuno, and S. Fujita, Jpn. J. Appl. Phys. **46**, 7217 (2007).
33) F. B. Zhang, K. Saito, T. Tanaka, M. Nishio, and Q. X. Guo, J. Cryst. Growth **387**, 96 (2014).
34) T. Terasako, H. Ichinotani, and M. Yagi, Phys. Status Solidi C **12**, 985 (2015).
35) S. Rafique, L. Han, and H. Zhao, Phys. Status Solidi A **213**, 1002 (2016).
36) S. Rafique, L. Han, M. J. Tadjer, J. A. Freitas, Jr., N. A. Mahadik, and H. Zhao, Appl. Phys. Lett. **108**, 182105 (2016).
37) H. Murakami, K. Nomura, K. Goto, K. Sasaki, K. Kawara, Q. T. Thieu, R. Togashi, Y. Kumagai, M. Higashiwaki, A. Kuramata, S. Yamakoshi, B. Monemar, and A. Koukitu, Appl. Phys. Express **8**, 015503 (2015).
38) X. Du, W. Mi, C. Luan, Z. Li, C. Xia, and J. Ma, J. Cryst. Growth **404**, 75 (2014).
39) N. M. Sbrockey, T. Salagaj, E. Coleman, G. S. Tompa, Y. Moon, and M. S. Kim, J. Electron. Mater. **44**, 1357 (2015).
40) S. Rafique, L. Han, A. T. Neal, S. Mou, J. Boeckl, and H. Zhao, Phys. Status Solidi A **215**, 1700467 (2018).
41) N. Kaminski, Proc. EPE, 2009.
42) B. J. Baliga, *Fundamentals of Power Semiconductor Devices* (Springer, New York, 2008).
43) Web [http://www.tamura-ss.co.jp/en/products/gao/index.html].
44) J. E. Hogan, S. W. Kaun, E. Ahmadi, Y. Oshima, and J. S. Speck, Semicond. Sci. Technol. **31**, 065006 (2016).
45) J. Yang, F. Ren, R. Khanna, K. Bevlin, D. Geerpuram, L.-C. Tung, J. Lin, H. Jiang, J. Lee, E. Flitsiyan, L. Chernyak, S. J. Pearton, and A. Kuramata, J. Vac. Sci. Technol. B **35**, 051201 (2017).
46) Web [https://www.3m.com/3M/en_US/company-us/all-3m-products/˜/3M-Fluorinert-Electronic-Liquid-FC-40/?N=5002385+3290667380&rt=rud].

© 2018 The Japan Society of Applied Physics